16th World Conference on Earthquake, 16WCEE 2017
Santiago Chile, January 9th to 13th 2017
Paper N° 1020
Registration Code: S-Z1461789796

VALIDATION OF NEAR-FAULT GROUND MOTION SIMULATIONS WITH DIRECTIVITY PULSES FOR USE IN ENGINEERING APPLICATIONS

S. Rezaeian[(1)], C. Lenon[(2)], S. Pei[(3)], P. Deng[(4)]

[(1)] *Research Civil Engineer, U.S. Geological Survey, Golden, CO, srezaeian@usgs.gov*
[(2)] *Student Intern, U.S. Geological Survey, Golden, CO, conorlenon@gmail.com*
[(3)] *Department of Civil and Environmental Engineering, Colorado School of Mines, Golden, CO, spei@mines.edu*
[(4)] *Department of Civil and Environmental Engineering, Colorado School of Mines, Golden, CO, pdeng@mines.edu*

Abstract

Due to the scarcity of recorded data for damaging near-fault earthquake ground motions with forward directivity pulses, engineers need simulations of such motions. However, before simulations can be used with confidence in engineering practice, they must be independently validated. In this paper, we use the stochastic simulation model of Dabaghi and Der Kiureghian [1] to generate synthetic near-fault pulse-like ground motions for recordings from the 1994 Northridge earthquake. We demonstrate how these simulations can be validated for engineering applications by comparing the fit of simulated to recorded elastic response spectra, using a newly proposed similarity index (SI). We then show how the simulations can be improved to obtain a better similarity index. The simulation model includes predictive equations for each model parameter in terms of easily accessible input variables for design such as earthquake magnitude, distance, and site specifications. We first use these predictive equations to estimate the model parameters, which are based on the global earthquake database used by Dabaghi and Der Kiureghian [1], to generate our first set of simulations. Then, we use estimates of site-specific model parameters to generate a second set of simulations and demonstrate the improvements in the SI. Finally, we improve the site-specific parameters by also considering the fit of simulations in terms of the response spectrum, which was not directly considered in [1], and generate a third set of simulations. The second and third sets of simulations can be used for site-specific analyses, where more detailed information is available at a site and more accurate ground motion simulations are required.

Keywords: near-fault simulation, directivity pulse, ground motion simulation and validation

1. Introduction

Near-fault ground motions can show forward directivity effects that are identified by long-period velocity pulses in their time-series and can cause large and damaging structural responses. This happens when seismic waves travel in the direction of the fault rupture and the velocity of the shear waves are very close to the rupture velocity. As the fault ruptures, new shear waves will act additively with the already propagating shear waves and cause a pulse-like energy release at sites located at the end of the fault. A two-sided velocity pulse will appear in the ground motion time-series, which will cause a spike in the long-period range of the response spectrum. This in turn causes larger demands on long-period structures such as tall buildings and bridges.

Due to scarcity of recorded near-fault ground motions, engineers need ground motion simulations with near-fault directivity pulses to accurately capture their effects on structural responses. Some deterministic physics-based simulations are able to generate the near-fault directivity effects; however, very few stochastic simulation approaches have this capability. One of the few examples of such stochastic models is the model of Dabaghi and Der Kiureghian [1], which provides predictive equations for the directivity pulse and the residual time-series in terms of easily accessible input variables for a design engineer (e.g., magnitude and distance). Dabaghi and Der Kiureghian [1] identified their model parameters empirically by fitting the statistical characteristics of a stochastic process with a velocity pulse to those of recordings from a global database of near-fault earthquake motions. These statistical characteristics capture the amplitude and rate of change (with respect to time) of the intensity and frequency content of a ground motion wave-form. A direct fit to the elastic response spectrum was not considered. Predictive relations were then developed through regression for each model parameter (i.e., parameters that describe the directivity pulse and the residual time-series) in terms of earthquake and site characteristics such as the earthquake magnitude, distance, and site specifications.

We use this model [1] to simulate near-fault recordings from the 1994 Northridge earthquake with a moment magnitude of 6.69 at 6 sites with distances ranging from 5.43 to 8.44 km. In order to demonstrate how near-fault simulations can be validated and to show how they can be improved for site-specific analysis, we approximate the model parameters in three different ways: 1) First, we use the predictive equations of [1] to estimate the model parameters and refer to them as the "global parameters" because the predictive equations were based on a global database of recordings. The drawback of a global model is that the convenience in prediction of parameters by using the earthquake and site characteristics, limits the accuracy of the simulations. 2) Then, we use the "site-specific parameters", which were identified in [1] for each record prior to developing predictive equations, to generate a second set of simulations and demonstrate the improvements in the simulated response spectra. 3) Finally, we also consider the fit of simulations to the elastic response spectra to generate a set of "improved site-specific parameters", resulting in a third set of simulations, and demonstrate how one can arrive at such improved values for any ground motion time-series. At each step, we quantify the improvements in the simulations using a response spectrum similarity index (SI), developed as part of another on-going research project [2]. This SI considers differences in both amplitude and slope of the response spectrum.

2. Simulation Model of Dabaghi and Der Kiureghian

In this paper, the stochastic simulation approach of Dabaghi and Der Kiureghian [1] is used, which generates the directivity pulse and the residual motion separately. Their method simulates the residual motion (i.e., the motion after removal of the directivity pulse) based on the model of Rezaeian and Der Kiureghian [3], which is a filtered white-noise process with the filter having a time-varying frequency content. The parameters that define the residual motion are I_a, D_{5-95}, D_{0-5}, D_{0-30}, t_{mid}, f_{mid}, f', ζ, t_0, and f_c. I_a is the Arias intensity, D_{5-95} is the significant duration of motion from 5 to 95% of Arias intensity (followed by 0 to 5% and 0 to 30%, respectively corresponding to D_{0-5} and D_{0-30}), t_{mid} is the time at the middle of strong shaking phase taken as the time at 30% Arias intensity of the residual motion, f_{mid} is the filter frequency at t_{mid}, f' is the rate of change of the frequency with time, ζ is the filter damping ratio, t_0 is the largest time with 0 Arias intensity, and f_c is the corner frequency for post-processing (see [3]). The directivity pulse is then simulated separately. The parameters that define the pulse are V_p, T_p, γ, ν, and $t_{max,p}$. V_p and T_p are the pulse amplitude and period, γ is the number of oscillations in the velocity time-series of the pulse, ν is the phase angle, and $t_{max,p}$ is the time of the peak of the envelope.

Dabaghi and Der Kiureghian [1] estimated the values of the model parameters for a global database of near-fault recorded ground motions by matching the evolution of intensity and frequency content of the recordings. They then developed predictive equations for each model parameter, P_i, i=1,…,15, by performing regression on the variables shown in Eq. (1). These predictive variables are F, an identifier for the fault mechanism (Northridge motions have a reverse fault mechanism); M_w, the earthquake moment magnitude; Z_{tor}, the depth from the surface to the top of the fault rupture (5.0 km for Northridge); R_{rup}, the closest distance to the fault rupture from the station; d, the distance along the fault to the site measured from the epicenter; V_{S30}, the shear wave velocity in the top 30 m of soil at the site; and θ_d, the angle in a vertical plane between the fault rupture plane and the direction between the hypocenter and the site. The variability for each model parameter and their correlations are represented by the normally distributed random errors, ϵ_i, with zero means and constant standard deviations.

$$P_i = \mathrm{f_i}\left(\mathrm{F}\,, M_w, Z_{tor}, R_{rup}, \mathrm{d}, V_{S30}, \Theta_d\right) + \epsilon_\mathrm{i} \tag{1}$$

2.1 Identification of model parameters in this study

The simulations in this study are generated for recordings from the 1994 Northridge earthquake. Northridge demonstrated the effects that pulse-like ground motions could have on structures and revealed the need to consider pulse-like behavior in seismic design. For each recording in our database, we estimate the model parameters in three ways: 1) "Global parameters" are calculated using the predictive equations given in [1] and shown in Eq. (1). 2) "Site-specific parameters" are taken from [1], where they were calculated for each specific record by matching the evolutionary intensity and frequency content of the simulations to recordings. 3) "Improved site-specific parameters" are estimated by also considering the fit of simulations to the elastic response spectrum.

3. Recorded Ground Motion Database

Our database of recorded near-fault ground motions with pulse-like behavior consists of 12 horizontal components at 6 recording stations recorded during the 1994 Northridge earthquake. The components are in x and y horizontal directions, representing the largest pulse direction and its orthogonal direction, respectively, as defined in [1]. The stations are listed in Table 1, along with the predictive variables, R_{rup}, d, V_{S30}, and θ_d for each site.

Table 1 – Recording stations and predictive parameters

Record	Full Station Name	R_{rup}, km	d, km	V_{S30} m/s	θ_d, °
JEM	Jensen Filtration Plant Generator	5.43	19.4	526	13.7
JFP	Jensen Filtration Administrative	5.43	19.4	373	13.7
NWP	Newhall – W Pico Canyon Road	5.48	19.4	286	11.0
PAR	Pardee – SCE	7.46	19.4	326	0.8
RRS	Rinaldi Receiving Station	6.5	19.4	282	18.3
VAN	LA Sepulveda VA Hospital	8.44	17.3	380	26.0

4. Similarity Index for Response Spectra of Simulations and Recordings

The simplest approach to validate an individual simulation for most engineering applications is by visual inspection of the elastic response spectra because most engineering demand parameters are mainly influenced by the spectral ordinates at fundamental periods of the structure. The drawback is that this method is not automated and therefore not scalable to a large number of simulations. In another on-going project [2], we developed a similarity index in order to emulate as much of the visual inspection process as possible, while allowing for efficient evaluation of a large number of simulations.

There are many ways to formulate a similarity index. In this paper, we focus on the amplitude and slope differences between response spectra. The amplitude similarity index, $SI_{amplitude}$, measures the amplitude difference between the simulated and recorded acceleration response spectra in a certain period range. The slope similarity index, SI_{slope}, measures how similar the slope of the simulated spectrum is to that of recorded motion in the same period range. The total similarity index, SI, is a combination of the two, as shown in Eq. (2)

$$SI = \sqrt{SI_{amplitude}^2 + SI_{slope}^2} \tag{2}$$

$SI_{amplitude}$ is calculated as follow

$$SI_{amplitude} = \bar{\varepsilon}/\beta \tag{3}$$

where,

$$\bar{\varepsilon} = \frac{1}{n}\sum_{i=1}^{n}\left(S_{a,s}(T_i) - S_{a,r}(T_i)\right) \tag{4}$$

and

$$\beta = \max\left|S_{a,s}(T_i) - S_{a,r}(T_i)\right| \tag{5}$$

$S_{a,s}(T_i)$ and $S_{a,r}(T_i)$ are the acceleration response spectral values of the simulation and recording at period T_i, respectively. The scalar n is the number of considered periods in a selected range. SI_{slope} is calculated as follow

$$SI_{slope} = \frac{\sum_{i=1}^{n}(T_i - \bar{T})(\varepsilon(T_i) - \bar{\varepsilon})}{\sum_{i=1}^{n}(T_i - \bar{T})^2} / \mu \tag{6}$$

where,

$$\mu = \frac{max|(T_i - \bar{T})(\varepsilon(T_i) - \bar{\varepsilon})| \times n}{\sum_{i=1}^{n}(T_i - \bar{T})^2} \tag{7}$$

and

$$\bar{T} = \frac{1}{n}\sum_{i=1}^{n} T_i \tag{8}$$

$\varepsilon(T_i)$ is the difference between $S_{a,s}(T_i)$ and $S_{a,r}(T_i)$. The slope and amplitude similarity indexes each have a range of [-1, 1], where a value closer to 0 represents a better fit. We use 5 period ranges in this study with a discretization of 0.005 sec. Each period range is denoted by $SI_{T_1-T_n}$: $SI_{0.1-5}$ covers most of the spectral range, $SI_{0.6-2.5}$ and $SI_{0.6-5}$ are the two ranges considered in [2] for analyzing a concrete frame structure with fundamental periods of 0.60 and 1.15 sec, $SI_{0.2-1}$ covers the period range for the majority of typical building structures between one and five stories tall, and SI_{1-3} covers the most common range of pulse presence (determined by visual inspection of recordings considered in this study) and is the sensitive range for softer and taller structures.

4.1 Similarity index modification

The main disadvantage of the above similarity index is that positive and negative differences across periods in the amplitude can cancel out to falsely indicate a good similarity index for a poor fit. An example is shown in Fig. 1, where a relatively poor simulation (gray) shows a good similarity index of 0.088 because it overestimates the recorded motion (black) for some periods, but underestimates it for other periods. Because of the definition of amplitude error in Eq. (4), the overestimation cancels out the underestimation, resulting in a SI close to zero.

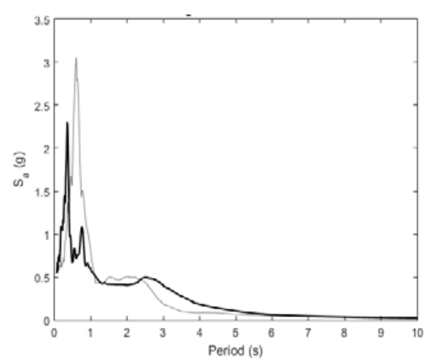

Fig. 1 – Response spectra. An example of a poor simulation with a good similarity index of 0.088 for T=[0.1, 5].

To address this issue, we modify the amplitude error and instead take the absolute value of the amplitude difference. This is done by replacing Eq. (4) with Eq. (9) as shown below.

$$\bar{\varepsilon} = \frac{1}{n}\sum_{i=1}^{n}\left|S_{a,s}(T_i) - S_{a,r}(T_i)\right| \tag{9}$$

One disadvantage of the above equation is that it removes any indication of whether the simulation is in general an over- or an under-estimation. In order to have a correct estimate of the amplitude of the similarity index, but not lose all the information obtained from the sign, the previous two variations are combined, i.e., Eq. (9) is used to determine the amplitude, while the sign from Eq. (4) is used to determine the over- or under-estimation.

$$SI = [sign]\sqrt{SI_{amplitude}^2 + SI_{slope}^2} \tag{10}$$

where, $[sign]$ comes from Eq. (4), but $SI_{amplitude}$ and SI_{slope} are calculated using the error in Eq. (9).

4.2 Shortcoming of the similarity index

Even with the modifications in Eq. (9) and Eq. (10), the similarity index still has a shortcoming in that it does not indicate how much the simulation over- or under-estimates the recorded motion. This shortcoming is demonstrated in Fig. 2. Fig. 2a shows a simulated response spectrum in gray, which is an overestimation of the real spectrum in black. Fig. 2b shows a simulated response spectrum that overestimates the real spectrum for some periods and underestimates it for other periods. For both cases, the similarity index is approximately equal to 0.1. Without seeing the figures, this may lead to the misunderstanding that the two simulations are “off” by approximately the same amount, and are both more of an overestimation than they are an underestimation. However, the simulation in Fig. 2a is an overestimation at almost every point, while the simulation in Fig. 2b is only an overestimation in the $T = [0.5, 1.2]$ and $T = [2, 3]$ ranges. Despite this issue, by using the modified similarity index, we can obtain a better similarity index value for simulations that are visually closer to the real records as will be shown later in this paper.

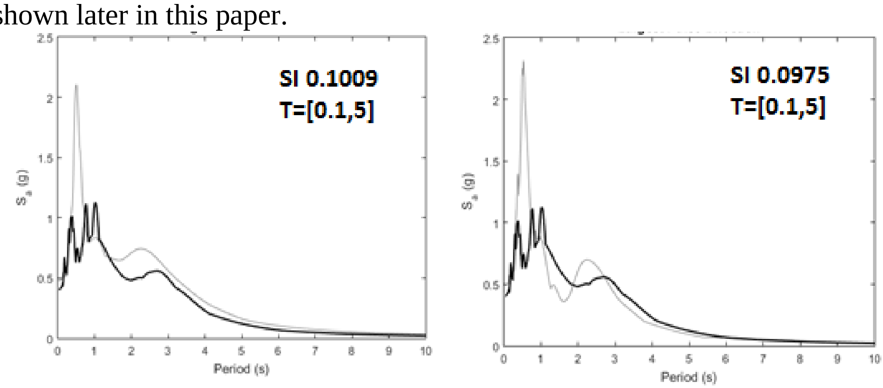

(a) (b)

Fig. 2 – Simulations with similar SIs, but different fits, a) over-estimation, b) over- and under-estimation.

5. Simulations Using Global Parameters

The global parameters for the pulse and residual motion are obtained from the predictive equations in Eq. (1), provided in [1]. Their mean values are given in Table 2. Note that we cap ω' at a maximum value of 0 (only negative or zero values), because based on the arrival of typical seismic waves we expect the frequency content of the time-series to decrease with time, i.e., high-frequency P-waves arrive first, followed by lower-frequency S-waves, and the very low-frequency surface waves. In our simulations, $f_c = 0.1252$, $t_0 = 0$, and $t_{mid} = D_{0-30}$. The pulse parameters for the y-direction are zero since there is no pulse in this direction (see [1] for more details).

Table 2 – Mean values of global estimates of the model parameters

Record	Pulse Parameters					Residual Motion Parameters						
	$\overline{V}_p$	$\overline{T}_p$	$\bar{\gamma}$	$\bar{\nu}$	$\overline{t}_{max,p}$	$\overline{I}_a$	$\overline{D}_{5-95}$	$\overline{D}_{0-5}$	$\overline{D}_{0-30}$	$\overline{f}_{mid}$	$\overline{f'}$	$\bar{\zeta}$
JEM X	72.2	1.6	2.3	1.0	4.3	.360	9.5	2.9	4.6	4.2	-.075	.199
JFP X	76.6	1.8	2.3	.896	4.3	.384	11.4	3.0	4.5	4.1	-.077	.207
NWP X	78.4	1.8	2.3	1.0	4.3	.365	12.1	3.1	4.4	3.6	-.068	.238
PAR X	69.9	2.0	2.3	1.1	4.8	.310	12.2	3.3	4.8	3.8	-.086	.223
RRS X	71.6	2.2	2.3	1.1	4.7	.409	11.4	3.3	4.8	3.8	-.069	.213
VAN X	64.1	1.9	2.3	.988	4.9	.286	10.9	3.2	4.9	4.1	-.090	.202
JEM Y						.395	9.1	3.0	4.6	4.3	-.083	.257
JFP Y						.406	10.3	3.0	4.4	3.9	-.077	.200
NWP Y						.403	11.7	3.2	4.5	3.7	-.060	.217
PAR Y						.307	12.5	3.4	5.0	4.0	-.114	.203
RRS Y						.340	12.2	3.3	4.9	3.9	-.081	.219

VAN Y						.311	10.4	3.7	5.0	3.9	-.073	.202

Table 3 – $SI_{0.1-5}$ values for simulations with the global parameters

Record	SI in x	SI in y
JEM	0.264	0.213
JFP	0.271	0.272
NWP	0.248	0.212
PAR	0.275	0.245
RRS	0.319	0.257
VAN	0.255	0.218

Using the predictive equations in [1], we randomize the mean values provided in Table 2 to generate 70 simulations for each record component. This number was chosen to achieve convergence of the similarity index. The $SI_{0.1-5}$ values (averages of 70 simulations for each record component) are given in Table 3. Fig. 3 shows response spectra of simulations for station VAN in the y-direction and for station JFP in the x-direction. These are examples of a relatively good and a relatively poor similarity index, respectively.

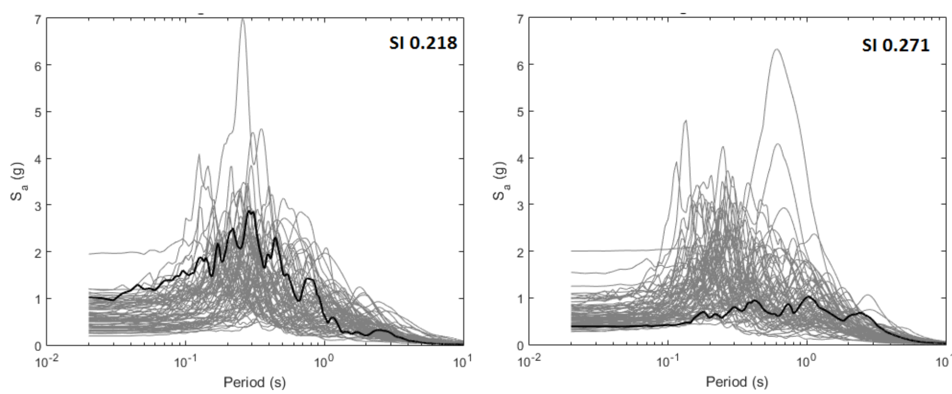

(a) (b)

Fig. 3 – Response spectra of simulations (gray) and recordings (black). a) Station VAN in the y-direction with a good fit (lower SI). b) Station JFP in the x-direction with a poor fit (higher SI).

6. Simulations Using Site-Specific (Record-Specific) Parameters

The site-specific parameters for pulse and residual motion are obtained from [1], which were estimated for each individual record by matching the evolutionary intensity and frequency content of the simulation and the recorded ground motion. These values are given in Table 4. Note that, similar to the global parameters, f' is capped at 0, f_c is set to 0.1252, and the pulse parameters for the y-direction are zero. Using the site-specific parameters in Table 4, we generate 70 simulations for each record component. The $SI_{0.1-5}$ values are given in Table 5. Fig. 4 shows example response spectra of simulations and recordings for station VAN and NWP, both in the x-direction. These are examples of a relatively good and a relatively poor fit, respectively, with SIs 0.098 and 0.374.

Table 4 – Site-specific estimates of the model parameters

Record	Pulse Parameters					Residual Motion Parameters								
	V_p	T_p	γ	ν	$t_{max,p}$	I_a	D_{5-95}	D_{0-5}	D_{0-30}	t_{mid}	f_{mid}	f'	ζ	t_0
JEM X	64.3	2.8	2.5	1.3	3.4	0.214	8.6	2.6	4.1	6.1	3.8	-0.12	0.1	0.6
JFP X	81.7	2.8	2.2	1.8	3.8	0.198	15.9	2.3	3.2	5.3	2.1	-0.08	0.1	0.9
NWP X	53.2	2.5	2.4	1.2	4.7	0.087	11.5	3.5	4.7	4.4	1.9	-0.08	0.16	0.2
PAR X	85.3	1.1	2.3	1.9	5.9	0.135	10.5	3.6	5.9	6.1	3.2	0	0.8	0.4
RRS X	118.6	1.2	2.2	0.6	2.3	0.357	9.7	1.7	3.2	3.8	5.4	-0.02	0.11	0.4

VAN X	77.1	0.9	2.1	0.7	2.4	0.710	8.5	2.3	4.1	3.3	4.2	-0.04	0.09	1.2
JEM Y						0.734	5.5	2.4	5.1	6.1	2.9	0	0.09	0.6
JFP Y						0.529	5.9	2.4	3.3	5.3	1.8	-0.01	0.08	0.9
NWP Y						0.100	8.8	2.8	4.6	4.4	1.4	-0.04	0.09	0.2
PAR Y						0.175	8	3.3	4.7	6.1	3.7	0	0.63	0.4
RRS Y						0.480	9	1.5	3	3.8	3.8	0	0.13	0.4
VAN Y						0.292	10	2.3	4.3	3.3	4.1	-0.06	0.19	1.2

Table 5 – $SI_{0.1-5}$ values for simulations with the site-specific parameters

Record	SI in x	SI in y
JEM	0.189	0.279
JFP	0.234	0.232
NWP	0.374	0.323
PAR	0.311	0.317
RRS	0.190	0.195
VAN	0.098	0.218

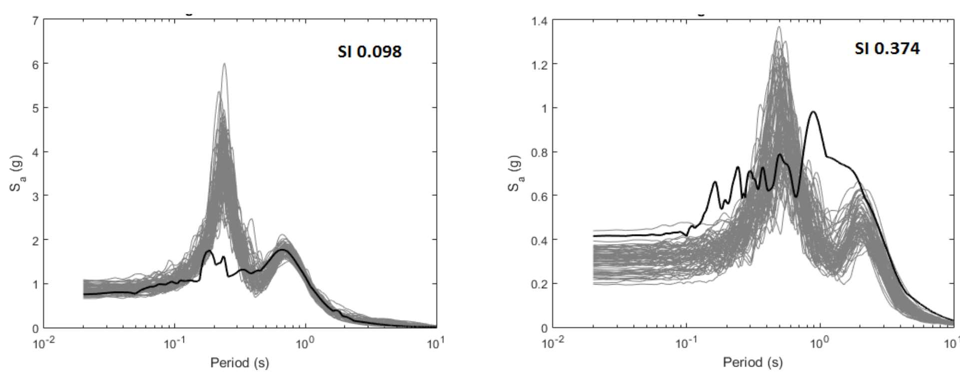

(a) (b)

Fig. 4 – Response spectra in the x-direction of stations a) VAN with a good fit, and b) NWP with a poor fit.

6.1 Improvements in the response spectra

The percent improvement in the similarity index for using site-specific parameters instead of global parameters is shown in Table 6. Negative values indicate diminishing quality of simulations, while positive values indicate improvement. The average overall improvement across the simulations for $SI_{0.1-5}$, which is a very long period range, is 0.394%. Of the 12 record component simulations, 6 show a worse $SI_{0.1-5}$, while 6 show improved values. Of the 6 pulse-like simulations, 2 got a worse $SI_{0.1-5}$, while 4 were improved. In terms of the improvement of the overall fit, this information could be misleading because the similarity index discretization is linear, which means that the period range from 1 to 5 sec accounts for 80% of the $SI_{0.1-5}$ values, whereas in visual inspection the period range from 1 to 5 sec is in the logarithmic scale and looks small compared to the rest of the spectrum. For this reason, it is beneficial to also look at the similarity index for other period ranges.

Table 6 also shows percent improvements in SI for two other shorter period ranges, namely, $SI_{0.6-2.5}$ and $SI_{0.2-1}$. These shorter period ranges could be more useful for engineering applications, depending on the fundamental periods of the structures. The average improvement for $SI_{0.6-2.5}$ is 10.3%, and the average improvement for $SI_{0.2-1}$ is 5.4%. We expected to see most improvements in the period ranges close to the pulse period, T_p, which is around 1 to 3 sec for our records, and it is the focus of improvements in the site-specific parameters because of the large spike it causes in the response spectrum.

Table 6 – Improvement in SI using site-specific parameters, compared to global parameters

Record	$SI_{0.1-5}$	$SI_{0.6-2.5}$	$SI_{0.2-1}$

	% ΔSI x	% ΔSI y	% ΔSI x	% ΔSI y	% ΔSI x	% ΔSI y
JEM	28.38	-31.15	21.3	-8.2	-0.89	-0.05
JFP	13.50	14.67	5.3	13.2	4.3	15.3
NWP	-50.91	-53.12	-12.3	1.2	-16.2	-7.7
PAR	-13.09	-29.38	19.0	-4.5	11.8	-12.2
RRS	40.38	24.10	55.0	0.6	10.5	28.5
VAN	61.48	-0.11	10.1	23.2	44.9	-13.6

Simulations with the most improved $SI_{0.1-5}$ correspond to station VAN in the x-direction, shown in Fig. 5. Observe that the shape of the simulated spectra is more clearly defined with site-specific parameters and there is less variability. The directivity pulse happens around 0.7 sec for all simulations, providing an overall good fit to the real response spectrum around the pulse period. There is still room for improvement, however, specifically in the amplitude and predominant frequency of the peak spectra, as will be discussed later.

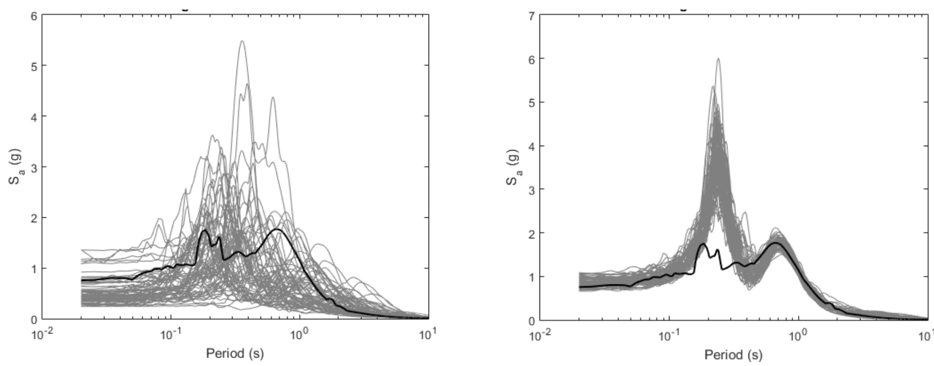

(a) (b)

Fig. 5 – Recorded (black) and simulated (gray) spectra for station VAN in the x-direction. a) Global simulations, b) Site-specific simulations.

Simulations with the least improved $SI_{0.1-5}$ correspond to station NWP in the y-direction, shown in Fig. 6. While we see some improvement in the range from 0 to 1 sec, the site-specific simulations largely underestimate the spectrum from 1 to 4 sec range, causing the average similarity index to reflect a poor fit. On the other hand, the global simulations slightly overestimate the spectra from 1 to 4 sec due to the larger variability of the model parameters, leading to an overall better similarity index for the global simulations. This is an example where the site-specific simulations have improved the visual fit to the response spectrum, but this improvement is not reflected in the similarity index.

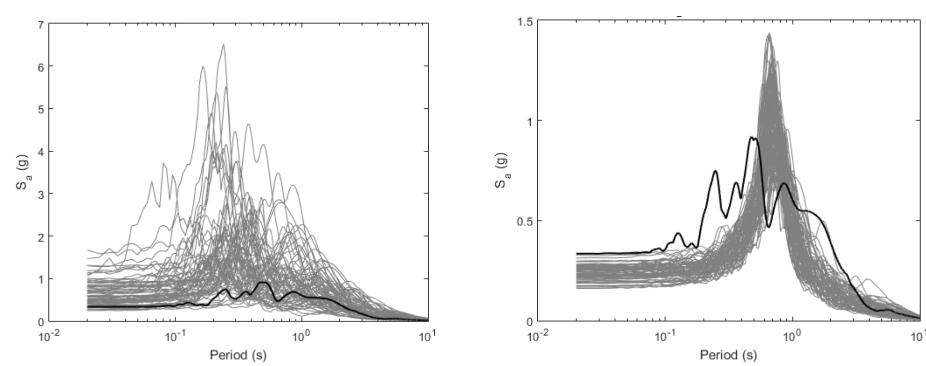

(a) (b)

Fig. 6 – Recorded (black) and simulated (gray) spectra for station NWP in the y-direction. a) Global simulations, b) Site-specific simulations.

7. Simulations Using Improved Site-Specific Parameters

As previously mentioned, the site-specific parameters were estimated by fitting the evolutionary intensity and frequency content of the simulations to recordings. It was assumed (based on previous studies) that this method would also provide a reasonably close match to the response spectrum, but a direct fit to the response spectrum was not considered in [1]. Because response spectrum is such an important characteristic in engineering applications, one could improve the site-specific parameters by also considering the direct fit of simulations to the response spectra of recorded motions in addition to the fit of evolutionary intensity and frequency content.

The first step in this "optimization" is determining the exact values of I_a, D_{5-95}, and t_{mid}, using the recordings. We calculated these values for the records in our database and confirmed that they were equal (or very close) to the values obtained from Eq. (1). Next, the frequency and bandwidth parameters, i.e., f_{mid}, f', and ζ, are optimized on a record by record basis, using the values of the site-specific parameters as initial guesses and updating them step-by-step (as will be described below) until a better fit to the response spectrum is achieved. The process described below is on a trial and error basis, but one could generate an automated procedure, using optimization algorithms, to obtain these improved parameters in future studies.

7.1. Improving the site-specific f_{mid} and f'

As previously mentioned, f_{mid} and f' represent the predominant frequency of the motion (equivalent to the frequency of the peak of the response spectrum) and the rate of change of the frequency in time, respectively. A higher f_{mid} will shift the peak response to a shorter period, while lower values will shift the peak to longer periods. These two parameters, introduced in [3], are related to the cumulative count of zero-level up-crossings (when the time-series crosses the zero-axis from below). According to [3], if the cumulative count of zero-level up-crossings is plotted against time, f_{mid} can be represented by the smoothed instantaneous slope of the resulting curve at t_{mid}, and f' can be estimated as the curvature of the parabolic shaped plot. An example is shown in Fig. 7, where the stars are used as matching points to fit a second degree polynomial (blue) to approximate f_{mid} and f'. In this example, the polynomial is very close to a straight line, suggesting a constant frequency (i.e., zero curvature and thereby zero f').

This type of plot along with that of the response spectra can be visually analyzed to determine if the site-specific values of f_{mid} and f' should be improved. If the fitted polynomial has a negative curvature, f' should be negative, reflecting a decreasing frequency. If the fitted polynomial has a positive curvature, f' will be a positive number, but will be capped at 0, reflecting a nearly constant frequency. If the fitted polynomial seems to underestimate the negative curvature of the target plot, then the initial value of f' should be modified to be more negative.

The site-specific value of f_{mid} is modified according to the location of the peak response in the response spectrum plot (Fig. 7b), where $T_{peak} = 1/f_{mid}$. Therefore, if the peak is located at 0.5 sec, f_{mid} should be set equal to 2 Hz. The average slope of the curve in Fig. 7a can then be estimated to further justify and adjust the new value of f_{mid}. For the example in Fig. 7, the slope of the target line is approximately $(47-7)/(50-3) \sim 0.85$. Additionally, the polynomial is very close to being linear, aside from the initial negative curvature from 0 to 8 sec. From the response spectrum in Fig. 7b, it is apparent that f_{mid} must decrease to shift the peak of simulations to the right. Therefore, we decrease f_{mid} from 1.8 to 0.95 (which is close to 0.85 than 1.8, but will give a more accurate visual location for the peak response compared to 0.85). f' is decreased slightly from -0.01 to -0.06 to capture a slightly more negative curvature.

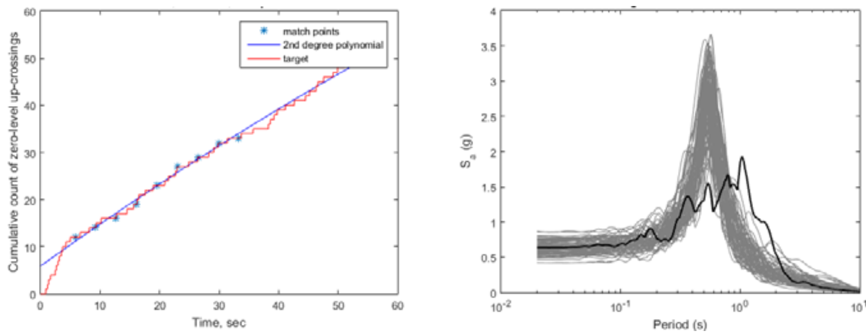

(a) (b)

Fig. 7 – a) Cumulative zero-level up-crossings in the acceleration time-series for JFP in y. b) Response spectra of site-specific simulations (gray) and recorded motion (black) of JFP in y.

7.2. Improving the site-specific ζ

The ζ parameter, introduced in [3], ranges between 0 and 1 and represents the bandwidth of the motion, which can also reflect how "wide" or "narrow" the peak of the response spectrum is. A higher ζ will result in a response spectrum with a "wider-bandwidth". Therefore, if simulations have consistently narrower bandwidths, ζ must be increased, and vice versa. An example of a low ζ value is shown in Fig. 8a, where the simulated bandwidths are narrower than the real record. Increasing the ζ value for simulations will reduce this discrepancy.

The parameter ζ can be approximated by taking the slope of the cumulative number of positive-minima and negative-maxima as described in [3]. This is shown in the example of Fig. 8b, where the black line represents the recorded motion and other colors represent simulations with various ζ values ranging from 0.1 to 0.9. The average slope of the black line is closest to that of the line corresponding to $\zeta = 0.2$. Therefore, we increase ζ from 0.09 to 0.2. ζ can vary with time, however, as shown by the 0 slope in the 0 to 4 sec range, the higher slope in the 4 to 6 sec range, and slopes alternating between zero and nonzero from 6 sec onwards. But for simplicity, as suggested in [3], a constant value that represents the average behavior over time is sufficient for simulations.

Using the combination of the two plots shown in Fig. 8, we are able to evaluate if the site-specific value of ζ provided in the previous section needs modification. First, the response spectra in Fig. 8a should be considered to determine if ζ needs adjustment. Then, the plot in Fig. 8b should be considered to justify and quantify the change by comparing the slopes of the lines.

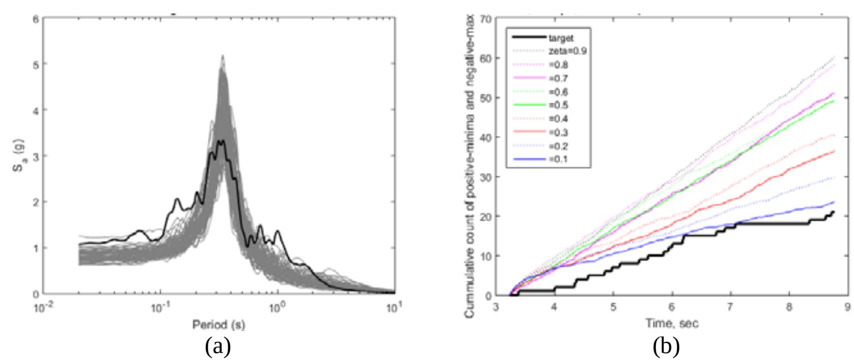

(a) (b)

Fig. 8 – a) Response spectra, JEM-y. b) Cumulative count of positive-minima and negative-maxima, JEM-y.

7.3 Improved Site-Specific Parameters

For each record in our database, the plot of the cumulative count of zero-level up-crossings, the plot of the cumulative count of positive-minima and negative-maxima, and the plot of response spectra are used to determine if the site-specific values of f_{mid}, f', and ζ need to be adjusted. The changes to these three parameters are shown in Table 7. Minor modifications to other model parameters (e.g., slightly modifying the pulse period, based on the response spectra plots) were made that are not reported here due to space limitations, but are small enough that they are not consequential to our final results. These plots will be shown in our presentation, demonstrating the reasoning for the change in each parameter.

Table 7 – Improved site-specific parameters, f_{mid}, f', and ζ

Record	Final values		
	f_{mid}	f'	ζ
JEM X	2.9	0	0.09
JFP X	1.0	-0.010	0.70
NWP X	1.4	-0.040	0.90
PAR X	3.7	0	0.90
RRS X	3.8	0	0.90
VAN X	5.0	-0.060	0.19
JEM Y	3.3	0	0.20
JFP Y	0.95	-0.060	0.30
NWP Y	1.9	-0.080	0.16
PAR Y	1.3	0	0.80
RRS Y	2.5	0	0.20
VAN Y	3.3	-0.020	0.20

7.4 Improvements in the Response Spectra

The percent improvements in $SI_{0.1-5}$, using the new simulations with improved site-specific parameters compared to both simulations with global parameters and simulations with site-specific parameters are given in Table 8. Compared to both previous sets of simulations, 5 of the 12 ground motions improved in terms of $SI_{0.1-5}$, with 3 of the 6 pulse-like motions improving. Table 9 shows the average overall improvement for all 12 record components for all 5 period ranges compared to simulations with the global parameters. From this table, it is apparent that most of the improvements occur for shorter period ranges ($SI_{0.6-2.5}$ and $SI_{0.2-1}$ are both positive, where the fundamental periods of most structures are and where the directivity pulses occur). The lack of improvement in the SI values for periods of 0.1 to 5 sec, 0.6 to 5 sec, and 1 to 3 sec is likely due to their long period ranges; they do not necessarily indicate a worst fit to the response spectrum (see Fig. 9) and may be reflecting the shortcomings of the chosen similarity index as was discussed earlier in the paper. The improved site-specific parameters further verify that most of the improvement happens in the 0.1 to 2.5 sec period range. To see each record's improvement, Fig. 9 shows the response spectra (average of 70 realizations) of simulations with the global, site-specific, and improved site-specific parameters for each record in the database.

Table 8 – Improvement in $SI_{0.1-5}$, using improved site-specific parameters

Record	% ΔSI (compared to global siml.)	% ΔSI (compared to site-specific siml.)
JEM X	27.17	-1.69
JFP X	-28.26	-48.27
NWP X	-35.31	10.34
PAR X	-12.38	0.63
RRS X	40.58	0.34
VAN X	42.40	-49.53
JEM Y	-15.20	12.16
JFP Y	-60.48	-88.07
NWP Y	-88.12	-22.85
PAR Y	-100.47	-54.94
RRS Y	17.44	-8.79
VAN Y	0.29	0.40

Table 9 – SI improvement for all period ranges compared to simulations with global parameters

SI Range		% ΔSI Site-Specific Parameters	% ΔSI Improved Site-Specific Parameters
Longer Period Ranges	$SI_{0.1-5}$	0.394	-17.7
	$SI_{0.6-5}$	10.4	-1.6
	SI_{1-3}	-4.4	-4.4
Shorter Period Ranges	$SI_{0.2-1}$	5.4	5.8
	$SI_{0.6-2.5}$	10.3	11.4

8. Conclusions

We used the stochastic simulation approach of Dabaghi and Der Kiureghian [1] to generate near-fault synthetic ground motions with directivity effects. We generated three different sets of simulations using global parameters, site-specific parameters, and improved site-specific parameters. The accuracy of simulations for engineering applications were measured in terms of the similarity of the elastic response spectra to recorded motions. We quantified this similarity by developing a similarity index, but also showed that this quantifiable measure can have some shortcomings. In general, the global simulations show more dispersion and the worst fit to recordings. This happens because global simulations represent the range of realizations from different events with identical source and site characteristics. Site-specific simulations show a better fit, but require more knowledge about parameters at the site. Finally, we demonstrated how the site-specific parameters can be further improved so that the simulations better match the response spectra of recordings and to improve SI.

9. Acknowledgment

We thank Dr. Mayssa Dabaghi for sharing her data and simulations with us and for providing valuable feedback.

10. References

[1] Dabaghi M and Der Kiureghian A (2014): Stochastic modeling and simulation of near-fault ground motions for performance-based earthquake engineering. *Technical Report PEER 2014*, Pacific Earthquake Engineering Research Center, Berkeley, USA.

[2] Deng P, Pei S, Hartzell S, Luco N, and Rezaeian S (2016): Correlation of ground motion spectrum shape to potential structural damage (Oral Communications, 2016).

[3] Rezaeian S and Der Kiureghian A (2010): Stochastic modeling and simulation of ground motions for performance-based earthquake engineering. *Technical Report PEER 2010*. Pacific Earthquake Engineering Research Center, Berkeley, USA.

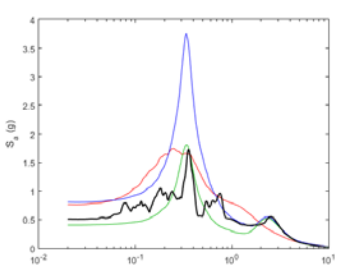

JEM X

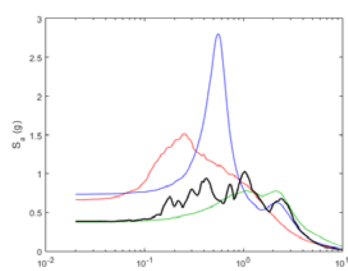

JFP X

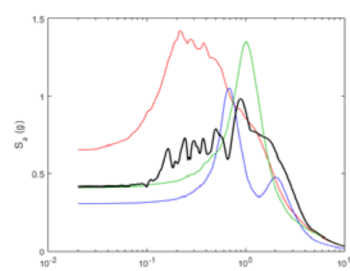

NWP X

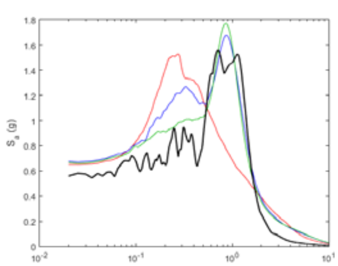

PAR X

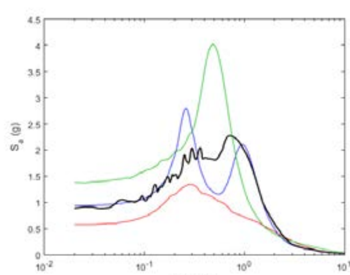

RRS X

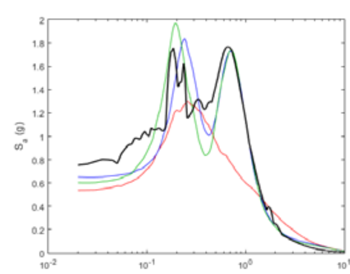

VAN X

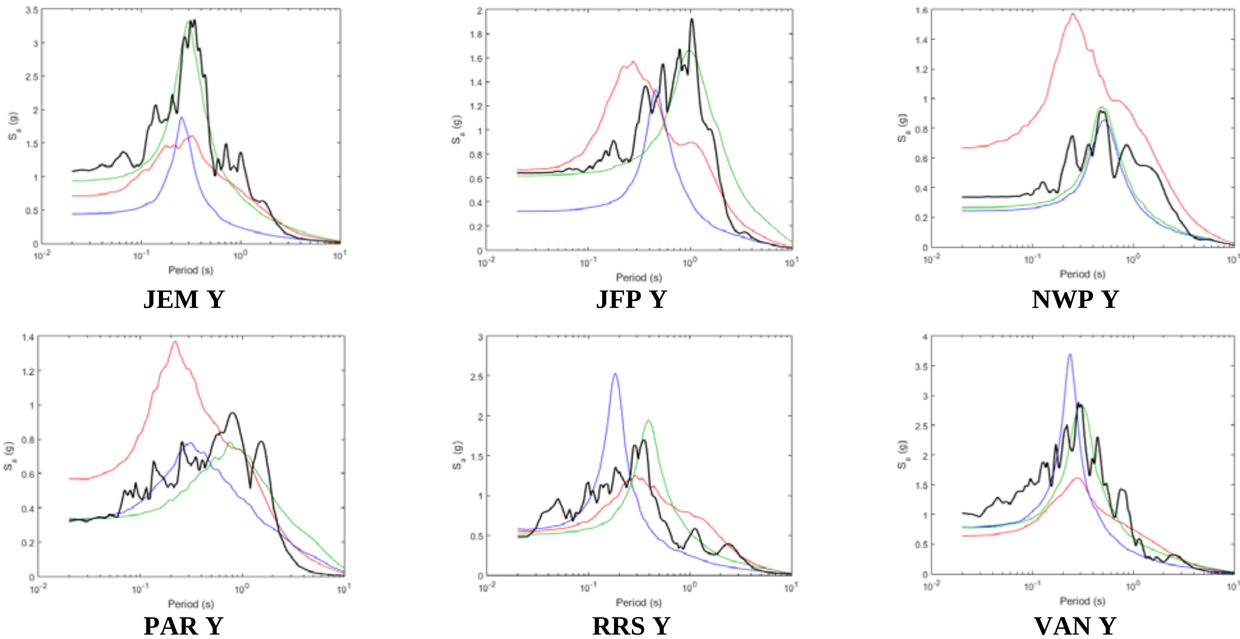

Fig. 9 – Mean response spectra of simulations with global (red), site-specific (blue), and improved site-specific (green) parameters compared to recorded spectrum (black)